Atmospheric Research 235 (2020) 104786

Contents lists available at ScienceDirect

Atmospheric Research

journal homepage: www.elsevier.com/locate/atmosres

Characteristics and source apportionment of $PM_{2.5}$ on an island in Southeast China: Impact of sea-salt and monsoon

Taotao Liu[a,b,c], Baoye Hu[a,b,c], Yuxiang Yang[e], Mengren Li[a,b], Youwei Hong[a,b,*], Xinbei Xu[b,c,d], Lingling Xu[a,b], Naihua Chen[e], Yanting Chen[a,b], Hang Xiao[a,b], Jinsheng Chen[a,b,*]

[a] Center for Excellence in Regional Atmospheric Environment, Institute of Urban Environment, Chinese Academy of Sciences, Xiamen 361021, China
[b] Key Lab of Urban Environment and Health, Institute of Urban Environment, Chinese Academy of Sciences, Xiamen 361021, PR China
[c] University of Chinese Academy of Sciences, Beijing 100086, PR China
[d] College of Resource and Environment, Fujian Agriculture and Forestry University, Fuzhou 350002, China
[e] Pingtan Comprehensive Experimental Area Environmental Monitoring Station, Pingtan 350400, China

ARTICLE INFO

Keywords:
$PM_{2.5}$
Source apportionment
Island
East Asian monsoon
Sea salt

ABSTRACT

To study the combined effects of the East Asian monsoon and ocean emissions on wintertime and summertime $PM_{2.5}$ in island cities, filter samples were collected simultaneously at four different functional sites. Based on the chemical compositions of $PM_{2.5}$, and positive matrix factorization (PMF) model analysis, the pollution characteristics and sources were determined. Insignificant differences, and some correlation in $PM_{2.5}$ reconstructed compositions were found among the sites ($P_{t\text{-test}} > 0.05$, $P > .05$), while significant differences, and no correlation, were found between winter and summer ($P_{ANOVA} < 0.05$, $P > .05$). There was more serious chloride depletion in summer (0.88 ± 0.05), caused by both significant Cl^- depletion and Na^+ enrichment, than in winter (0.18 ± 0.10). The concentrations of non-sea-salt-SO_4^{2-} in winter were close to those in summer, but the sulfate oxidation ratio (SOR) in winter was much lower than that in summer. The results could be explained by the fact that sea-salt-SO_4^{2-} has an important contribution to secondary inorganic aerosol on island cities. From both air trajectory clustering and PMF analysis, it was found that there was significant aerosol aging and regional transport in the island city during the East Asian monsoon, and that continental air masses control the variation of air pollution in winter, while sea breezes dominate the characteristics of $PM_{2.5}$ in summer. This study helps to understand the characteristics and source mechanisms of $PM_{2.5}$ pollution under complex meteorological conditions in island cities.

1. Introduction

With rapid economic development and urban agglomeration, fine particulate matter ($PM_{2.5}$) in East Asia has gradually developed characteristics such as wide-ranging regional pollution, complex formation mechanisms and explosive growth (Luo et al., 2017; Weagle et al., 2018). High concentrations of $PM_{2.5}$ affect air quality, atmospheric visibility, climate change and human health (Poschl, 2005; Zhou et al., 2016; Liu et al., 2016). Recently, pollution characteristics and sources of $PM_{2.5}$ were investigated not only for urban and suburban areas, but also for background or remote areas (Tao et al., 2014; Norris et al., 2014; Zhang et al., 2017; Wang et al., 2019). Haze development is predominantly caused by regional transport and local sources, and synoptic weather plays an important role in the evolution of haze in the East Asian continental outflow region (Seo et al., 2017; Yeh et al., 2017). Therefore, it is necessary to study further the interaction between air pollution and weather in these areas, especially in coastal cities (Li et al., 2017; Ding et al., 2017; Liu et al., 2018).

Air quality in subtropical coastal areas is influenced by the transport of pollution from East Asia during the monsoon season (Wang et al., 2019). Most previous studies relating to monsoons focused on the $PM_{2.5}$ concentration or gaseous species (Jeong and Park, 2017). The effects of northeasterly winds on the particle concentration and its size distributions in Bachok were analyzed, reflecting a mixture of local anthropogenic emissions, aging aerosol transported from East Asia and clean air masses from marine regions (Dominick et al., 2015). In addition, large differences in aerosol composition, including SO_4^{2-} concentrations and Cl^- depletion, were observed between marine air

* Corresponding author at: Center for Excellence in Regional Atmospheric Environment, Institute of Urban Environment, Chinese Academy of Sciences, Xiamen 361021, China.
E-mail addresses: ywhong@iue.ac.cn (Y. Hong), jschen@iue.ac.cn (J. Chen).

https://doi.org/10.1016/j.atmosres.2019.104786
Received 30 April 2019; Received in revised form 12 November 2019; Accepted 20 November 2019
Available online 21 November 2019

masses from the South China Sea and continental air masses affected by urban areas in East Asia (Farren et al., 2019). Higher nss-SO_4^{2-}, NH_4^+ and nss-SO_4^{2-}/NO_3^- ratios were found in marine aerosols over the South China Sea, compared to remote open oceans and the western Pacific Ocean (Hsu et al., 2007). Chou et al. (2008) suggested that the Asian outflow aerosols, in which SO_4^{2-} can be neutralized by NH_4^+, make NO_3^- more abundant in Taiwan, and the chlorine deficiency is mainly caused by the reaction of NaCl and HNO_3. Bagtasa et al. (2018) found that long-range transport accounts for around one-third of aerosol content in the Philippines, during the monsoon. However, the formation mechanism of $PM_{2.5}$ and internal and external influences in island cities of East Asia are still not fully understood.

Pingtan Island, located on the western side of the Taiwan Strait, is affected by the subtropical East Asian monsoon, sea and land breezes and typhoons. The monsoon wind flows from the subtropical ocean to the land in summer, while in winter the wind flows from the high-latitude continent to the ocean (Zhang et al., 2010; Jia et al., 2008; Webster et al., 1998). In our previous study, $PM_{2.5}$ concentrations in Pingtan occasionally appear to be high, up to 100 μg m^{-3}, resulting not only from the influence of local sources, but also from the contribution of the outflow from continental air pollutants (Hu et al., 2019). Pingtan offers an opportunity to study how the formation process and sources of $PM_{2.5}$ in an island area are controlled by the East Asian monsoon. Therefore, the aims of this study are: (1) to investigate the pollution characteristics of $PM_{2.5}$ on Pingtan Island during summer and winter; (2) to identify the potential sources of $PM_{2.5}$ using receptor modeling (PMF) and backward trajectories; and (3) to determine the impact of the monsoon and sea salt on the differences between winter and summer by integrating the chemical components of $PM_{2.5}$ and identifying their sources. The results provide a scientific basis and comprehensive understanding of the formation mechanisms of $PM_{2.5}$ in island cities of East Asia.

2. Materials and methods

2.1. Sampling

Based on geographical location, distribution of anthropogenic activities, and dominant meteorological conditions, four sampling sites on Pingtan Island (Fig. 1 and Table S.1) were selected: 36-Foot Lake (FL), Jinjing Bay (JB), Jun Mountain (BG) and County Government (CG) (details are shown in Table S1 and Fig. S1). FL is a suburban site, close to a natural freshwater lake, and surrounded by emissions from traffic and agricultural activity. JB, a developing town, is mainly affected by emissions from construction, shipping and traffic, with the sampling site located at the rooftop of a 21-storey building. BG, a background site on the island, is located halfway up the Jun Mountain, which suffers less impact from anthropogenic emissions. BG is surrounded to the northeast by mountains, resulting in a southwestward wind throughout the year. The site is not representative, so no specific analysis was done, and it was only used as a background reference. CG, a developed town, is influenced by emissions from urban traffic and food preparation. Due to the "channeling effect" of the Taiwan Strait, the wind speed in Pingtan is high throughout the whole year. The maximum wind speed can reach 19.7 m s^{-1} during the typhoon period. Generally, wind speeds in winter are higher than those in summer (except at BG), which is beneficial to the dispersion of air pollutants (Table S.1). Fig. S.1 shows wind rose plots for the four sites, by season. Apart from BG, southwestward and northeastward were the dominant wind directions for summer and winter, respectively. Daily $PM_{2.5}$ filter samples were collected (over 23 h, from 9:00 am to 8:00 am the next day), using two low-flow (5 L min^{-1}) air samplers (MiniVol, AirMetrics Corp., USA), in winter (from Jan. to Feb. 2017) and summer (from Jul. to Aug. 2017). Polycarbonate filters (Whatman, USA, 47 mm) were used to analyze metallic elements, while quartz filters (Whatman, USA, 47 mm) were used for water-soluble inorganic ions, organic carbon (OC) and elemental carbon (EC). In total, 50 sets of $PM_{2.5}$ samples (26 in winter and 24 in summer) and 4 sets of blank samples were collected at each site and strict quality control and assurance was applied to the measuring instruments throughout the sampling period. A schedule was applied to check the flow of the samplers and clean them regularly. We also regularly ran 2 or 3 samplers to start sampling at the same time and site, and the target compounds among these duplicate samples all differed by < 10%. In addition, different categories of air pollutant ($PM_{2.5}$, PM_{10}, NO_2, SO_2, CO, O_3) and meteorological parameters were measured at the monitoring sites.

2.2. Experiments

The mass concentrations of $PM_{2.5}$ were measured using the

Fig. 1. Location of Pingtan and the four sampling sites.

gravimetric method. Cations (Na^+, NH_4^+, K^+, $Ca^{2+}$and Mg^{2+}) and anions (F^-, Cl^-, NO_3^- and SO_4^{2-}) were measured using quartz filters via ion chromatography (883 Basic, Metrohm, Switzerland). EC and OC in $PM_{2.5}$ were measured using a thermal-optical transmittance (TOT) carbon analyzer (Sunset Model-4, USA), following the National Institute for Occupational Safety and Health (NIOSH) protocol. Secondary organic carbon (SOC, OC_{sec}) was estimated using the following formulas (Castro et al., 1999):

$$OC_{sec} = OC_{tot} - OC_{pri} \quad (1)$$

$$OC_{pri} = EC \times (OC/EC)_{min} \quad (2)$$

The elemental components of the $PM_{2.5}$ samples were analyzed using polycarbonate filters through wave dispersive X-ray fluorescence (WD-XRF) spectrometry (Axios-MAX, Panalytical, Holland). Thirteen elements (V, Mg, Al, Si, K, Ca, Ti, Mn, Fe, Cu, Zn, As, Pb) were measured. The methods are described in detail in our previous study (Du et al., 2017).

2.3. $PM_{2.5}$ mass reconstruction

$PM_{2.5}$ can be reconstructed into nine groups: organic matter (OM), elemental carbon (EC), non-sea-salt-SO_4^{2-} (nss-SO_4^{2-}), NO_3^-, NH_4^+, sea salt (SS), crustal elements (CE), trace elements (TE), and other (undetected) components.

The OM concentration was calculated by multiplying OC by a conversion factor. Based on OM oxidation, the OC multiplier was chosen within the range between 1.2 and 2.6. The multipliers of non-urban sites are expected to be highest, because of the level of oxidation and the conversion of secondary organic compounds during the process of transport (Chow et al., 2015; Jennerjahn, 2012). Therefore, 1.8 was chosen for BG and 1.6 for the other three sites in this study.

SS contains the components ss-Cl^-, ss-Na^+, ss-Ca^{2+}, ss-K^+, ss-Mg^{2+}, and ss-SO_4^{2-}. Assuming that all Na^+ is from SS, the concentrations of other species were calculated as ratios to Na^+, from the seawater chemistry: ss-Cl^- (1.8), ss-Ca^{2+} (0.038), ss-K^+ (0.036), ss-Mg^{2+} (0.12), ss-SO_4^{2-} (0.252) (Li et al., 2017). The concentration of SS was then derived from:

$$SS = Na^+ + Cl^- + ss - Ca^{2+} + ss - K^+ + ss - Mg^{2+} + ss - SO_4^{2-} \quad (3)$$

where symbols refer to the concentration of the respective species. The concentrations of nss-SO_4^{2-}, NO_3^-, NH_4^+, and chemical elements (including EC) can be determined directly. The concentration of CE was derived using the sum of oxides method (Andrews et al., 2011):

$$CE = 2.14Si + 1.89Al + 1.43Fe + 1.4nss - Ca + 1.2nss - K + 1.67Ti \quad (4)$$

again, symbols refer to the concentration of the respective species. The concentration of TE was defined as the sum of the concentrations of As, Mn, Pb, Cu, Zn, V and nss-Mg. Lastly, “other components” was defined as the remaining portion of $PM_{2.5}$ and includes F^-.

2.4. Data quality control and statistical analysis

Every filter was equilibrated at a temperature 25 ± 0.1 °C and relative humidity (RH) 52 ± 2%, and then weighed on an electronic microbalance (Sartorius 0.01 mg, Germany). The water used for pre-treatment of the sample was ultra-pure (resistance coefficient > 18 MΩ cm). The method detection limits (MDLs) for F^-, Cl^-, NO_3^-, SO_4^{2-}, Na^+, NH_4^+, K^+, Ca^{2+} and Mg^{2+} were 0.05, 0.03, 0.02, 0.02, 0.19, 0.19, 0.15, 0.31, and 0.45 μmol L^{-1}, respectively. When measuring the concentrations of water-soluble ions, a point concentration of 10 ppm of standard solution was tested for every 10 samples and the correlation coefficient of the standard curve applied to these tests should be > 0.995. The linear fitting results between the anions and cations showed that the slopes were 0.86–0.90 and R^2 > 0.93 in both winter and summer. Thirteen elements (V, Mg, Al, Si, K, Ca, Ti, Mn, Fe, Cu, Zn, As, Pb) were detected, with detection limits of 3.0×10^{-4}–5.4×10^{-2} μg cm^{-3}. In this study, every 10 samples was inserted a duplicate sample for quality control. The measurement error of repeated analysis results of ions and elements was controlled in 10%, while the measurement error of $PM_{2.5}$ was in 5%. Recovery experiments of standard addition of ions and elements were tested for three groups, and the recoveries were 108 ± 20%, indicating that the sampling and the results of the chemical composition analysis in this study were reliable. Standard samples of various water-soluble ions were purchased from the National Standard Material Center; NIST SRM 2783 Standard material was used for quality control for the analysis of metal elements. Field blanks were collected twice at every site by season during the sampling period, and were taken using the same procedures as for the $PM_{2.5}$ samples, but with the samplers switched off. At least three blank samples were tested for each batch of samples. Blanks were detected by the same procedures to correct real samples, by subtracting the blank values from sample concentrations.

2.5. PMF analysis

In this paper, the US EPA (United States Environmental Protection Agency) PMF 5.0 (positive matrix factorization) model was used to identify the sources of the $PM_{2.5}$ samples in Pingtan, and its equation is (Norris et al., 2014; Paatero and Tapper, 1994; Paatero, 1997):

$$X = GF + E \quad (5)$$

where X is the sample concentration matrix ($n \times m$, n is the sample number, m is the chemical composition number), G is the factor (pollutant source) contribution matrix ($n \times p$, p is the number of precipitation factors), F is the factor profile matrix ($p \times m$) and E is the residual matrix ($n \times m$), defined as:

$$e_{ij} = x_{ij} - \sum_{k=1}^{p} g_{ik} f_{kj} \quad (6)$$

$$Q(E) = \sum_{i=1}^{n} \sum_{j=1}^{m} \left(\frac{e_{ij}}{s_{ij}} \right)^2 \quad (7)$$

where s_{ij} is the standard deviation of X, and the elements in G and F are all non-negative. $Q(E)$ is one of the model criteria, and subsequent analysis can be carried out only when $Q(E)$ converges. The matrices G and F are determined when the optimization causes $Q(E)$ tend to the number of degrees of freedom.

The variables input to the PMF model in this study include the daily average concentration of OC, EC, SO_4^{2-}, NO_3^-, NH_4^+, Na^+, Cl^-, K^+, Ca^{2+}, Mg^{2+}, Fe, Si, Al, Cu, Zn, Pb, Mn, Ti, As and V in $PM_{2.5}$. The number of each species was 187, meeting the operational requirements of PMF. Data inputs of PMF included the concentrations and uncertainties, and the uncertainties were calculated in detail from (Li et al., 2018; Polissar et al., 1998):

$$uij = \sqrt{(EF \times conc.)^2 + (MDL)^2} \quad (8)$$

where EF is the error factor based on experience, ~10–20%, and MDL is the minimum detection limit of chemical concentration. However, when the concentrations were lower than the MDL, they were replaced by half the MDL, and the uncertainties were defined as 5/6 of the MDL. The signal-to-noise ratios (S/N) were > 1.0 for the 19 species (except V), and they were defined to be “strong” (Paatero and Hopke, 2003); V was re-weighted as “weak” because the concentrations of a third of the samples were less than the MDL.

Based on experience and reference files, six to eight factors were tested. We compared the lowest $Q_{robust}/Q_{expected}$ at each step increase in number of factors (Brown et al., 2015). Table S.2 shows that there was a decrease (0.64) in $Q_{robust}/Q_{expected}$ going from six to seven factors and a larger decrease (0.71) going from seven to eight factors. When changes

in $Q_{robust}/Q_{expected}$ become smaller with increasing number of factors, this can indicate that too many factors are being fitted, suggesting that eight factors may be the optimal solution here. The displacement of the factor elements (DISP) had no swaps for all factors, indicating that the solutions had no data errors and were well defined. The bootstrap (BS) for results with eight factors showed one factor of 55% mapping, and 10% of BS-DISP runs were rejected due to factor swaps. However, with seven factors, one factor of the BS had 70% mapping and 0% of BS-DISP runs were rejected. Combining uncertainty and source profiles, seven factors were retained for Pingtan after numerous runs.

2.6. Analysis of the backward trajectories of air masses

The backward trajectories of air masses arriving Pingtan in two seasons during the campaign were simulated and clustered by using MeteoInfo (Wang et al., 2014). 24-h backward trajectories were run every hour, with starting time 0:00 and ending time 23:00 (local time), at 100 m height, and located at 25.50°E, 119.79°N. Meteorological data were provided by NOAA ARL (ftp://arlftp.arlhq.noaa.gov/pub/archives/gdas1).

2.7. Correlation and difference tests

The correlations and differences of chemical species among different sampling sites were investigated using Pearson correlation and paired sample *t*-tests, respectively. The method of paired sample t-tests must meet the condition that the differences between the pair-samples are normally distributed. The differences in source contributions among the trajectory clusters and between winter and summer were examined using an ANOVA test.

3. Results and discussion

3.1. Overview of $PM_{2.5}$ concentration and chemical compositions

Table 1 shows the comparison of $PM_{2.5}$ concentrations and their chemical components in this study, and at other major coastal cities worldwide. Similarly to Seoul, Mexico and Barcelona, the masses of $PM_{2.5}$ in Pingtan were lower than in Xiamen, Fuzhou, Lin'an, Qingdao and Hong Kong, and higher than in Penghu, Toronto and Yokohama (Heo et al., 2009; Elizabeth et al., 2004; Querol et al., 2004; Zhang et al., 2012; Li et al., 2016; Zhang et al., 2017; Cao et al., 2012; Lee et al., 2003; Khan et al., 2010). In these studies, SO_4^{2-}, NO_3^- and NH_4^+ (SNA) were the predominant components, ranging from 25.2% to 46.3%. Apart from Haikou, the concentrations of NO_3^- were higher than those of NH_4^+ in Chinese cities (Table 1), while two other cities (Mexico and Yokohama) showed the reverse pattern (Liu et al., 2017; Elizabeth et al., 2004; Khan et al., 2010). The higher NO_3^- has been explained by the rapid increase in the number of vehicles in recent years. OM was also an important component of $PM_{2.5}$. The OM concentrations in the Chinese cities ranged from 14.9% to 31.9%, while the OM concentrations in other countries ranged from 21.8% to 62.4%. The lowest EC concentration was observed in Pingtan, followed by Toronto, indicating limited primary emissions impacts (Lee et al., 2003). Most previous studies have shown clear seasonal variations in $PM_{2.5}$, especially for winter and summer, whereas this is not seen in suburban areas in Pingtan (Fig. 2) (Li et al., 2018; Wang et al., 2016; Zhang et al., 2017). $PM_{2.5}$ concentrations were observed at the different sampling sites in the following order: JB (37.52 ± 16.26 μg m^{-3}) > BG (37.10 ± 15.02 μg m^{-3}) > FL (33.71 ± 9.99 μg m^{-3}) > CG (29.73 ± 16.25 μg m^{-3}). BG has the lowest wind speed (1.93 ± 1.61 m s^{-1}) and few local sources, so its second highest $PM_{2.5}$ concentration indicates regional transport and accumulation of air pollutants. This analysis of seasonal and site variation makes it possible to correlate the results with the influence of meteorological conditions and anthropogenic factors.

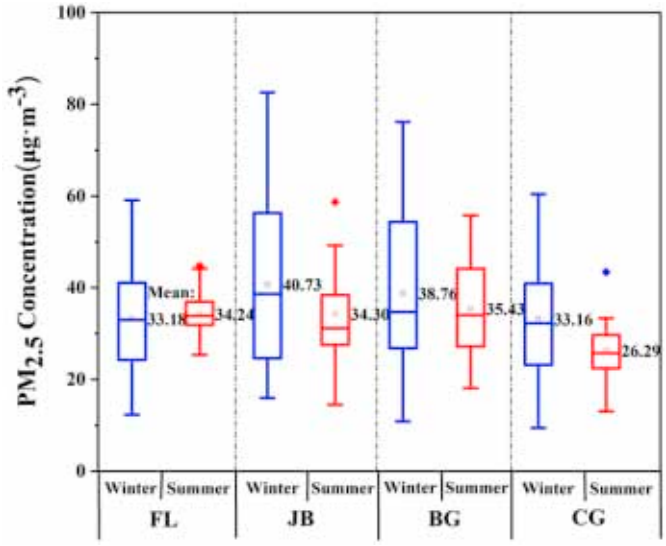

Fig. 2. Distribution characteristics of $PM_{2.5}$ in Pingtan, by season.

As shown in Fig. 3(a), the OC and EC contributions to the $PM_{2.5}$ concentration were higher in winter than in summer. Unlike inland cities, Pingtan has no industry and does not require heating for warmth

Table 1
Comparison of chemical components in $PM_{2.5}$ in coastal areas (μg m^{-3}); locations in China except where otherwise stated).

Location	Sampling-period (YY/MM)	$PM_{2.5}$	SO_4^{2-}	NO_3^-	NH_4^+	OM	EC	Reference
Fuzhou (FL)	17/01–17/02, 17/07–17/08	33.7	6.0	3.0	1.4	7.2	0.4	This study (2019)
Fuzhou (JB)		37.5	9.1	3.3	1.6	5.6	0.4	This study (2019)
Fuzhou (BG)		37.1	5.7	2.7	1.3	7.0	0.3	This study (2019)
Fuzhou (CG)		29.7	6.4	3.4	1.7	6.0	0.4	This study (2019)
Haikou	15/01,15/05,15/07,15/09	23.3	4.7	1.6	1.7	5.3	1.6	Liu et al. (2017)
Xiamen	09/06–10/05	86.2	11.2	6.0	4.5	27.5	3.0	Zhang et al. (2012)
Fuzhou	13/07–15/04	53.6	8.0	5.3	4.2	12.8	2.0	Li et al. (2016)
Penghu	13/07–15/04	23.6	3.9	2.1	0.9	4.6	1.1	Li et al. (2016)
Lin'an, Ningbo	2014–2015	68.9	16.9	9.2	5.8	17.4	2.7	Zhang et al. (2017)
Qingdao	03/01, 03/06–03-07	134.8	21.6	18.9	14.8	41.8	5.4	Cao et al. (2012)
Hong Kong	03/01, 03/06–03-07	88.4	21.2	9.7	7.1	22.1	6.2	Cao et al. (2012)
Seoul, Korea	03/03–06/12	37.6	5.8	5.2	3.7	11.4	2.9	Heo et al. (2009)
Mexico City, Mexico	2000–2002	35.1	5.9	2.7	3.0	21.9	8.4	Elizabeth et al. (2004)
Toronto, Canada	00/02–01/02	12.7	2.3	1.8	1.2	4.4	0.5	Lee et al. (2003)
Barcelona, Spain	1999–2001	27.6	4.2	2.3	2.0	12.2	NA	Querol et al. (2004)
Yokohama, Japan	07/09–08/09	20.6	3.8	1.0	2.3	4.5	1.9	Khan et al. (2010)

NA = data not available

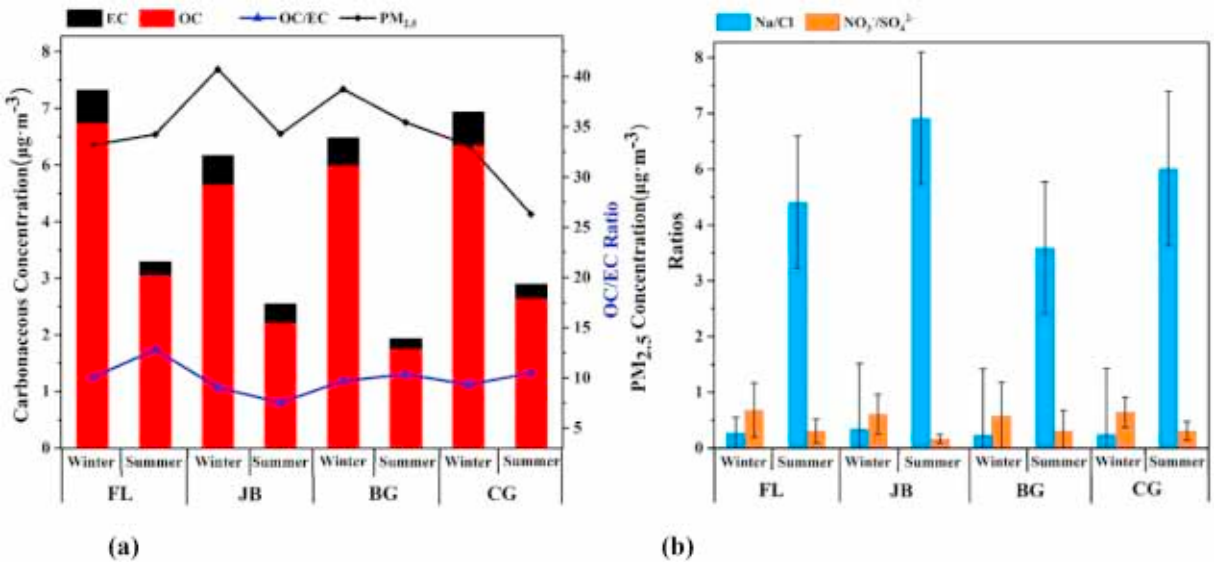

Fig. 3. Distribution characteristics of OC, EC and their concentration ratio (a); the ratios [Na]/[Cl] and $[NO_3^-]/[SO_4^{2-}]$ at four sites, by season (b).

in winter. The reason for the higher winter contributions is the dominant meteorological conditions, especially the East Asian monsoon (Zhang et al., 2013). These mean mainly northward winds and the Continental Asian Outflow leads to higher OC and EC concentrations in winter. Previous studies indicate that the ratio of OC to EC from coal combustion and biomass burning is estimated to be 8, while that from vehicle exhausts is estimated to be 4 (Safai et al., 2014; Shi et al., 2011; Watson et al., 2001; Zhao et al., 2013). In both summer and winter, the ratios of OC to EC in Pingtan are higher than 8 (Fig. 3(a)), showing that OC and EC come mainly from coal combustion and biomass burning. These results illustrate the importance of the regional transport. The percentage of POC (primary organic carbon) and SOC were calculated using Eqs. (1,2), as described in Section 2.2. SOC accounted for 70–90% of the total, suggesting the influence of aged aerosols. The aged aerosols could be associated with photochemical reactions of primary organic matter and regional transport. In winter, the predominant northeastward wind brought more aged aerosols through the outflow of continental pollutants to the monitoring sites, while strong oxidation conditions in summer can enhance the formation of aged aerosols in an island area (Liu et al., 2016a). In this study, the ratio $[NO_3^-]/[SO_4^{2-}]$ was higher in winter than in summer at all four sites, based on the seasonal distribution characteristics shown in Fig. 3(b). High concentrations of nitrate aerosol in the YRD region of China could elevate the concentrations of related air pollutants in coastal area of southeast China through long-range transport (Zhang et al., 2007). A previous study also found NO_3^- over East Asia in winter to significantly enhance NO_3^- concentrations in the downwind regions as far as the Pearl River Delta (PRD) region of China (Ying et al., 2014).

The conversion efficiencies of NO_2 to NO_3^- and SO_2 to SO_4^{2-} were calculated from the formulas NOR = $[NO_3^-]/([NO_3^-] + [NO_2])$ and SOR = $[SO_4^{2-}]/([SO_4^{2-}] + [SO_2])$, respectively (Table S.3). The saturation of secondary transformation means NO_2 and SO_2 were negatively or non-correlated with NOR and SOR in Pingtan (Yin et al., 2014). Limited NO_2 and low concentrations of NO_3^- (winter: 3.39 μg·m^{-3}; summer: 1.31 μg·m^{-3}) in Pingtan made NOR in winter (0.27 ± 0.14) higher than that in summer (0.22 ± 0.13). The concentrations of nss-SO_4^{2-} in winter (6.77 μg·m^{-3}) and summer (6.65 μg·m^{-3}) are close, while SOR in winter (0.55 ± 0.12) was much lower than in summer (0.63 ± 0.13), which can be explained by the fact that sea-salt-SO_4^{2-} has a more important contribution to secondary inorganic ions on islands than inland and in coastal cities (Yin et al., 2014; Zhang et al., 2017). A previous study has shown that when SOR > 0.25 and NOR > 0.1, this is representative of high oxidation values. The higher the values are (Table S.3), the higher the conversion strength (Colbeck and Harrison, 1984).

In this study, Na^+ and Cl^- concentrations were higher in summer than in winter, indicating that a large amount of sea salt enters the atmosphere from the ocean under the influence of the predominant southeastward wind and waves. From the ratio of Na^+ to Cl^- (Fig. 3(b)), it can be seen that there was chloride depletion. The chloride depletion was estimated using the equation Cl^-_{dep} = ($[Na^+]$/0.56 − $[Cl^-]$)/$[Na^+]$ × 0.56 (Quinn et al., 2000). The chloride depletion in summer (0.88 ± 0.05) was larger than that in winter (0.18 ± 0.10). KCl and NaCl can form HCl by reacting with acidic gases (such as HNO_3), and then react with NH_4^+ in particulates; higher temperatures (Table S.1) in summer promote the volatilization of NH_4Cl, leading to a reduction in chlorine salt (Hu et al., 2008; Martens et al., 1973). Although relative humidity had a negative effect on chloride depletion through its impact on heterogeneous reactions, photochemical reactions played a more important role in chloride depletion, so that more intense chloride depletion occurred in summer (Hsu et al., 2007). The ratio of Na^+ to Cl^- concentrations in seawater is close to 0.557 (Wang and Shooter, 2001), and the concentration of Cl^- in $PM_{2.5}$ in winter showed a significant enrichment compared with this.

3.2. Inter-site and inter-seasonal analysis of $PM_{2.5}$ mass reconstruction

Table 2 shows the correlations and differences for chemical species of $PM_{2.5}$, between winter and summer and among sites FL, JB and CG. The compositions were mostly characterized by insignificant correlations (P > .05) and significant differences (P_{ANOVA} < 0.05) between winter and summer at each site. Large differences in meteorological parameters (including monsoon, air temperature, relative humidity, radiation and boundary layer dynamics) lead to varying pollution sources between winter and summer (Hsu et al., 2017; Poschl, 2005). For a small number of components, the difference between winter and summer is insignificant, showing that these pollution emissions have seasonal stability. The CE (Si, Al, Fe, nss-Ca, nss-K, Ti), EC and TE (As, Mn, Pb, Cu, Zn, V, nss-Mg) components are thought to represent dust, vehicle exhaust and industry emissions (Amato et al., 2009; Hueglin et al., 2005; Zhang et al., 2013; Cao et al., 2008). There are dense road traffic and ship emissions all year round at developing region JB, while CG, a residential region, is affected by local residential activities. Compared with other sites, the highest nss-SO_4^{2-} concentration (winter: 7.32 μg m^{-3}; summer: 10.26 μg m^{-3}) and proportion (winter: 17.63%; summer: 29.33%) at JB may be related to precursor emissions

Table 2
Correlation and difference for chemical species of $PM_{2.5}$ between winter and summer, among FL, JB and CG sites.

Species	Correlation[a]		Difference	Correlation		Difference	Correlation		Difference
Winter	R	P	P_{ANOVA}[e]	R	P	P_{ANOVA}	R	P	P_{ANOVA}
Summer[b]	FL			JB			CG		
EC	−0.367	0.240	0.000	−0.584	0.046	0.014	−0.069	0.830	0.000
OM	−0.193	0.549	0.001	−0.433	0.159	0.000	0.619	0.032	0.010
nss-SO_4^{2-}	0.153	0.635	0.003	0.005	0.987	0.323	0.283	0.372	0.004
NO_3^-	−0.099	0.761	0.000	−0.186	0.563	0.000	−0.394	0.205	0.000
NH_4^+	−0.201	0.531	0.001	−0.161	0.618	0.002	0.013	0.969	0.000
SS	−0.186	0.563	0.000	−0.107	0.741	0.004	0.033	0.920	0.000
CE	0.632	0.050	0.383	0.000	1.000	0.484	0.014	0.966	0.102
TE	0.222	0.537	0.039	−0.353	0.352	0.051	−0.245	0.443	0.152
Winter[c]	R	P	$P_{t\text{-}test}$[f]	R	P	$P_{t\text{-}test}$	R	P	$P_{t\text{-}test}$
	FL and JB			JB and CG			CG and FL		
EC	−0.039	0.904	0.744	−0.204	0.524	0.847	0.889	0.000	0.603
OM	−0.151	0.639	0.923	−0.129	0.690	0.654	0.771	0.003	0.153
nss-SO_4^{2-}	0.147	0.647	0.112	0.206	0.521	0.426	0.745	0.005	0.048
NO_3^-	−0.441	0.151	0.315	−0.378	0.226	0.956	0.739	0.006	0.030
NH_4^+	0.015	0.962	0.231	0.034	0.917	0.297	0.769	0.003	0.000
SS	0.054	0.868	0.756	0.134	0.678	0.172	0.519	0.083	0.028
CE	−0.403	0.248	0.052	−0.122	0.737	0.148	−0.327	0.327	0.003
TE	−0.298	0.474	0.559	−0.123	0.752	0.696	−0.242	0.501	0.476
Summer[d]	R	P	$P_{t\text{-}test}$	R	P	$P_{t\text{-}test}$	R	P	$P_{t\text{-}test}$
	FL and JB			JB and CG			CG and FL		
EC	0.919	0.000	0.001	0.906	0.000	0.009	0.923	0.000	0.062
OM	0.821	0.001	0.001	−0.019	0.954	0.363	0.188	0.558	0.573
nss-SO_4^{2-}	0.600	0.039	0.000	0.628	0.029	0.001	0.910	0.000	0.042
NO_3^-	0.724	0.008	0.228	0.882	0.000	0.145	0.648	0.023	0.819
NH_4^+	0.906	0.000	0.111	0.966	0.000	0.105	0.874	0.000	0.044
SS	0.147	0.649	0.378	0.349	0.266	0.156	0.615	0.033	0.954
CE	0.073	0.853	0.658	0.333	0.348	0.711	0.235	0.486	0.424
TE	0.343	0.211	0.169	−0.496	0.060	0.566	−0.167	0.553	0.833

[a] 2-tailed test of significance is used.
[b] Correlation and difference are analyzed at each site between winter and summer.
[c] Correlation and difference are analyzed between FL, JB and CG, in winter.
[d] Correlation and difference are analyzed between FL, JB and CG, in summer.
[e] Difference is analyzed by using an ANOVA test.
[f] Difference is analyzed by using a paired sample *t*-test.

(i.e., local industrial activities may emit SO_2).

Unlike the pair CG and FL, the correlations and differences between FL and JB, and JB and CG, are insignificant in winter ($P > .05$, $P_{t\text{-}test} > 0.05$). The correlations and differences between CG and FL can be divided into three groups. The first group has significant correlations ($P < .01$) and insignificant differences ($P_{t\text{-}test} > 0.05$). This group includes EC and OM, which are good tracers of incomplete combustion of fossil fuel and biomass burning in primary sources (Turpin and Huntzicker, 1995), and secondary transformation, respectively (Shi et al., 2011; Zhao et al., 2013). CG is ~3 km northeast of FL, and the prevailing wind direction at CG and FL is northeastward, which means that wind arriving at CG has passed through FL, having a regional impact. The second group was characterized by significant correlations ($P < .01$) and significant differences ($P_{t\text{-}test} < 0.05$), which are seen in nss-SO_4^{2-}, NO_3^- and NH_4^+. The concentrations of nss-SO_4^{2-}, NO_3^- and NH_4^+ at CG in winter were 6.85, 4.86, 2.59 μg m^{-3}, respectively, which were higher than those at FL (6.15, 4.02, 1.71 μg m^{-3}). These findings imply that there are similar secondary formation and short-range transport characteristics between FL and CG. The third group, consisting of SS and CE, was characterized by insignificant correlations ($P > .05$) and significant differences ($P_{t\text{-}test} < 0.05$). The CE include Si, Al, Fe, nss−Ca, nss-K and Ti, which could be emitted from coal combustion, industrial sources, biomass burning or dust. The pollution sources in urban and suburban areas were different, and agricultural activities occurred more frequently at FL. SS mainly includes Na^+ and Cl^-. Apart from marine sources, there are contributions from coal and wood combustion (Mcculloch et al., 1999; Morawska and Zhang, 2002), mineral dusts (Li and Shao, 2009; Sun et al., 2006) and garbage burning (Zárate et al., 2000) as the main sources of Cl^-. The proportion of SS of $PM_{2.5}$ is 7–13% in winter and 16–25% in summer. The Na^+ concentration in summer is around 10.9 times than that in winter (because of sea freezing), while the Cl^- in winter is around 2.16 times than that in summer (because of lower Cl^- depletion). The Cl^- concentration at FL (1.33 μg m^{-3}) is higher than that at CG (1.06 μg m^{-3}). Because many agricultural activities of straw burning and biomass burning are happened at suburban FL, there are additional sources of Cl^- at FL.

The Inter-site correlations and differences for SS, CE and TE in summer had $P > .05$, $P_{t\text{-}test} > 0.05$. Combining with the analysis above, it can be concluded that CE mainly represents dust in summer. However, dust may come from construction and road fugitive dust (Cesari et al., 2014; Han et al., 2007). Huang et al. (2017) indicate that soil dust is from long-range transport. The local construction and road dust lead to an insignificant correlation, and the regional transport leads to insignificant differences between sites. Similarly, for TE the combination of less industry-related activity and diffusion in small areas causes the same result. Hence, we cannot determine what the major controlling factor is. The Mg^{2+}/Na^+ mass ratio was 0.04 ± 0.01 in summer, which was lower than 0.12, the bulk seawater ratio (Hsu et al., 2007). This result indicates that the high chloride depletion in summer is caused by both Cl-depletion and Na^+ enrichment. An additional Na^+ source causes the insignificant correlation for SS. Partly significant correlations or differences mainly appear for EC and secondary components (OM, nss-SO_4^{2-}, NO_3^- and NH_4^+). Whether it is significant or insignificant depends on the dominant factor:

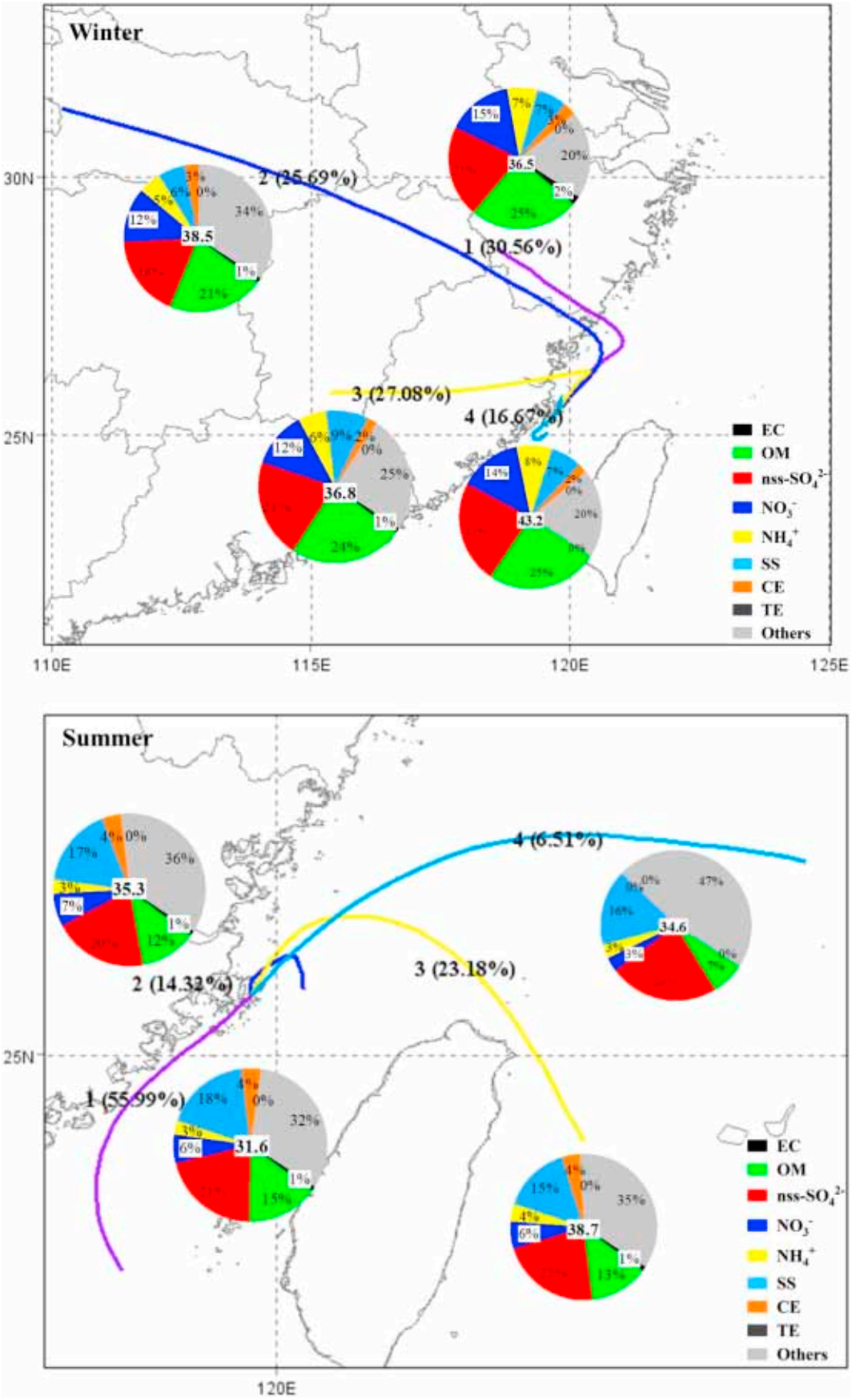

Fig. 4. Cluster results of air mass trajectories, relative contributions of chemical components and $PM_{2.5}$ concentrations of each air mass to the $PM_{2.5}$ concentrations, by season.

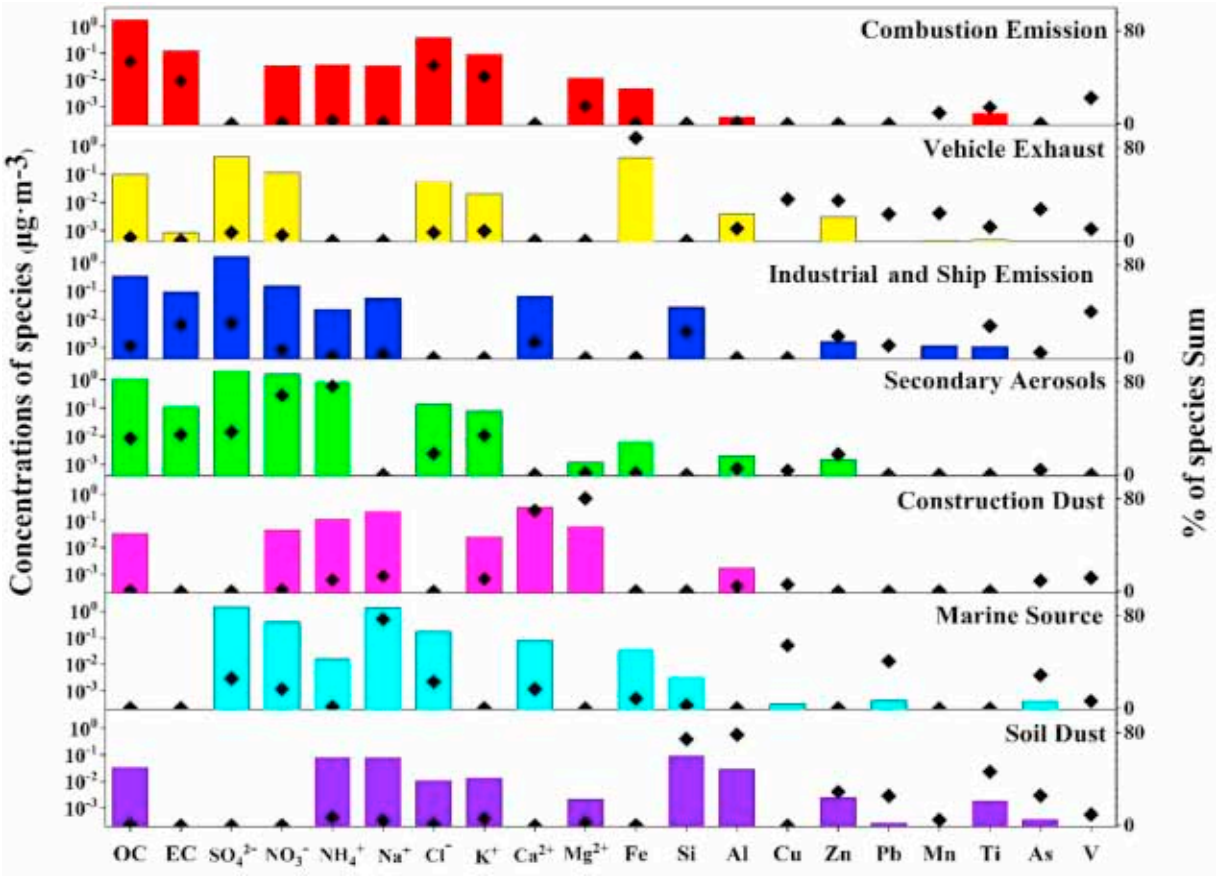

Fig. 5. PMF source profiles for $PM_{2.5}$ samples obtained during the sampling period.

precursor emissions or the extent of the regional transport.

3.3. Effect of the monsoon on $PM_{2.5}$

Pingtan, a subtropical and coastal city in southeastern China, has a climate affected by the shifting of Asian Monsoon system, which causes significant seasonal differences in meteorological conditions. In summer, there are subtropical high pressures, typhoons, heavy monsoon rains, and the monsoon blows from the Pacific Ocean (Bagtasa et al., 2018; Li et al., 2017). In contrast, air transported from inland China, coupled with a strong temperature inversion and low air pressure in winter, can be favorable for the accumulation of particulate matter (Wang et al., 2019; Wang et al., 2014; Zheng et al., 2018). The back trajectories of air parcels show a clear picture in the two sampling periods. Fig. 4 presents the cluster results of air mass trajectories and chemical components of $PM_{2.5}$ in winter and summer. The $PM_{2.5}$ concentrations are indicated at the centers of the pie charts. It can be seen that air masses mainly originated from inland in winter, while all air masses originated from the marine environment in summer.

In winter, Air Mass 1 had the highest proportion (30.56%) of the total, transmitted via a short pathway from Zhejiang province. Air Mass 2 (25.69%) traveled via a long pathway from the northwest, with smaller proportions of most components than in the other three air masses and larger proportions of CE and others. This result indicates that long-range transport leads to a decline in dust and complicates aerosol structures. Air Mass 3 (27.08%) arrived from the west, originating from Jiangxi province. The pathways of Air masses 1, 2 and 3 all originated in southeastern China and passed over the sea. Air Mass 4 (16.67%) originated in the Taiwan Strait, carrying the second highest $PM_{2.5}$ concentration (40.12 μg m^{-3}). In summer, the air masses arriving at Pingtan had mostly marine origins. Air Mass 1 (55.99%) originated in the Taiwan Strait. Air Mass 2 (14.32%) was transmitted from the Taiwan Strait but arrived by hooking northward in a counterclockwise direction. Air Mass 3 (23.18%) began at the outer rim of Taiwan and carried the highest $PM_{2.5}$ concentration of 38.7 μg m^{-3}. Air Mass 4 (6.51%) originated from the outer rim of East China Sea, carrying a low proportion of CE, TC and EC.

The average $PM_{2.5}$ concentration of each air mass in winter (38.7 μg m^{-3}) was close to that in summer (35 μg m^{-3}). The percentages of secondary pollutants accounted for 56–70% in winter and 36–45% in summer, and sea salt 15–18% in summer. Furthermore, significant differences ($P_{ANOVA} < 0.01$) in compositions of $PM_{2.5}$ reconstruction among the trajectory clusters were obtained. Pingtan has few local pollution sources, and pollution is mainly controlled by air mass trajectories, so these results indicate that there was significant aerosol aging and regional transport in the island city during the East Asian monsoon, and that continental air masses control the variation of air pollution in winter, while sea breezes dominate the characteristics of $PM_{2.5}$ in summer.

3.4. Source apportionment of $PM_{2.5}$

Figs. 5 and 6 present the PMF factor profiles and the contribution of various sources to $PM_{2.5}$. The high contributions of OC, EC, Cl^-, and K^+ appear in Factor 1; OC, EC, and Cl^- act as coal combustion tracers and OC, EC, and K^+ as biomass burning tracers (Xu et al., 2018; Li et al., 2018), indicating that there is a mixed source of coal combustion and biomass burning. Therefore, Factor 1 was identified as combustion emission. Factor 2 shows high contributions of Cu, Pb, Fe, Zn, Mn, Ti, As and V, which are generally indicators of vehicle exhaust. Cu, regarded as a good tracer of vehicle emissions, mainly originates from the wearing of tires and brakes (Amato et al., 2009), V originates mostly

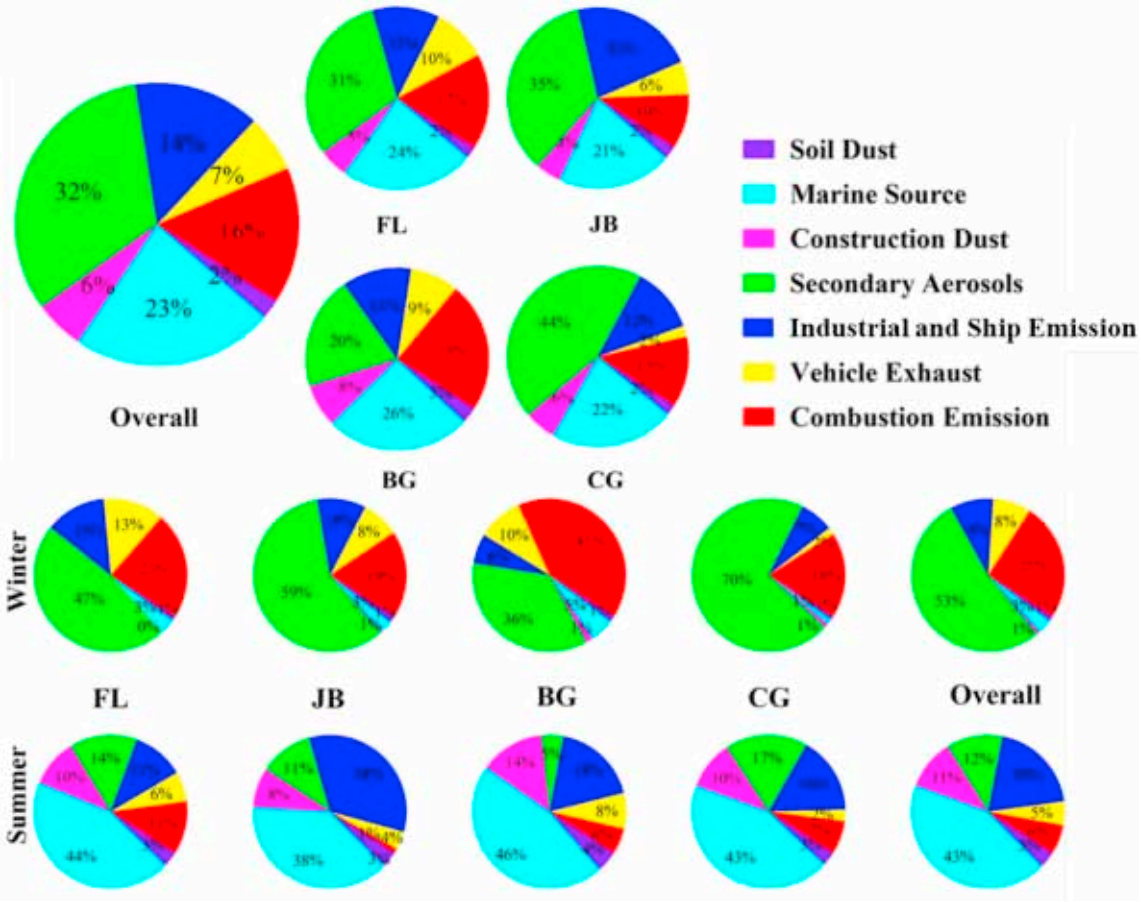

Fig. 6. Source contributions to $PM_{2.5}$ during the sampling period, by season and by site.

from heavy oil combustion (Hueglin et al., 2005), and the lubricant oil that is used in the tire manufacturing process and in brake linings contains a high concentration of Zn (Zíková et al., 2016). Factor 3, contributing a high loading of metal elements (Zn, Pb, As, V and Mn), was characterized by industrial and ship emission sources (Moffet et al., 2008). Factor 4 was associated with secondary aerosol, with high loads of SO_4^{2-}, NO_3^- and NH_4^+ (Song et al., 2006). Factor 5 was dominated by Ca^{2+} and Mg^{2+}, which are related to construction dust (Zhang et al., 2013). Factor 6, with the highest proportion of Na^+ loading, was associated with marine sources. Factor 7 was designated as crustal dust, and dominated by Al, Si, Ti, Zn, Pb and As (Cao et al., 2008).

As shown in Fig. 6, the contributions of various sources were similar among the four sites, but the differences between winter and summer were significant. Secondary formation was one of the largest sources and was five times larger in winter (55%) than in summer (12%). However, marine sources account for 43% in summer, and construction dust including high Ca^{2+} and Mg^{2+}, an important part of which comes from sea salt in island cities, accounts for 11%. These results are consistent with the air trajectory clusters in Section 3.3. Secondary aerosols were generated mainly from secondary transformations during transport in winter, and both sea salt and secondary products were dominant factors in summer. The contributions from combustion emission (25%) were larger in winter. There was little contribution from biomass burning and coal combustion in Pingtan, which can be attributed to monsoon convection in winter. JB had a higher loading from industrial and ship emissions (22%) than the other three sites (12%), which were affected by a mixture of local industry activities, port activities and regional transport.

Overall, secondary aerosol, marine sources and combustion emissions, which are defined as mainly controlled by regional transport in the above analysis, show a higher proportion in summer or winter. However, soil dust, construction dust, industrial and ship emissions, and vehicle exhaust, for which it is not clear if the dominant factor is local sources or regional transport, show relatively stable proportions across summer and winter.

4. Conclusions

The pollution characteristics and sources of $PM_{2.5}$ in Pingtan were investigated in order to determine the relative contributions between primary emissions and secondary formation, and between local sources and regional transport. For individual reconstructed compositions of $PM_{2.5,}$ significant differences and no correlations were found between winter and summer, and positive correlations and insignificant differences were observed among different sites. The predominant northeastward wind in winter brought more aged aerosols through the outflow of continental pollutants to the monitoring sites, while strong oxidation conditions and sea salt carried by waves in summer affected the formation of aged aerosols and marine contributions in the island area. There was more serious chloride depletion in summer than in winter, and the high chloride depletion in summer is caused by both significant Cl^- depletion and Na^+ enrichment.

Significant differences in compositions of $PM_{2.5}$ reconstruction among the trajectory clusters indicated that the elevated $PM_{2.5}$ concentrations in Pingtan are mainly controlled by air mass transport. In winter, three air masses were identified as originating mainly in southeastern China and passing over the sea, and one air mass as originating in the Taiwan Strait. In summer, the air masses arriving at Pingtan were mostly transmitted from marine regions and originated in the Taiwan Strait and the outer rim of the East China Sea. Overall, these

results indicate that there was significant aerosol aging and regional transport in an island city during the East Asian monsoon, and that while continental air masses control the variation of air pollution in winter, sea breezes dominate the characteristics of $PM_{2.5}$ in summer.

Declaration of Competing Interest

The authors declare that they have no known competing financial interests or personal relationships that could have appeared to influence the work reported in this paper.

Acknowledgments

This work was supported by the National Key Research and Development Program (2016YFE0112200&2016YFC02005); the National Natural Science Foundation of China (41575146); and the Chinese Academy of Sciences Interdisciplinary Innovation Team Project.

Appendix A. Supplementary data

Supplementary data to this article can be found online at https://doi.org/10.1016/j.atmosres.2019.104786.

References

Amato, F., Pandolfi, M., Escrig, A., Querol, X., Alastuey, A., Pey, J., Perez, N., Hopke, P.K., 2009. Quantifying road dust resuspension in urban environment by Multilinear Engine: a comparison with PMF2.0. Atmos. Environ 43, 2770–2780.

Andrews, E., Saxena, P., Musarra, S., Hildemann, L.M., Koutrakis, P., McMurry, P.H., Olmez, I., White, W.H., 2011. Concentration and composition of atmospheric aerosols from the 1995 SEAVS experiment and a review of the closure between chemical and gravimetric measurements. J. Air Waste Manage. Assoc. 50, 648–664.

Bagtasa, G., Cayetano, M.G., Yuan, C.-S., 2018. Seasonal variation and chemical characterization of $PM_{2.5}$ in northwestern Philippines. Atmos. Chem. Phys. 18, 4965–4980.

Brown, S.G., Eberly, S., Paatero, P., Norris, G.A., 2015. Methods for estimating uncertainty in PMF solutions: examples with ambient air and water quality data and guidance on reporting PMF results. Sci. Total Environ. 518–519, 626–635.

Cao, J.J., Chow, J.C., Watson, J.G., Wu, F., Han, Y.M., Jin, Z.D., Shen, Z.X., An, Z.S., 2008. Size-differentiated source profiles for fugitive dust in the Chinese Loess Plateau. Atmos. Environ. 42, 2261–2275.

Cao, J.J., Shen, Z.X., Chow, J.C., Watson, J.G., Lee, S.C., Tie, X.X., Ho, K.F., Wang, G.H., Han, Y.M., 2012. Winter and summer $PM_{2.5}$ chemical compositions in fourteen chinese cities. J. Air Waste Manage. Assoc. 62, 1214–1226.

Castro, L.M., Pio, C.A., Harrison, R.M., Smith, D.J.T., 1999. Carbonaceous aerosol in urban and rural European atmospheres: estimation of secondary organic carbon concentrations. Atmos. Environ. 33, 2771–2781.

Cesari, D., Genga, A., Ielpo, P., Siciliano, M., Mascolo, G., Grasso, F.M., Contini, D., 2014. Source apportionment of$PM_{2.5}$ in the harbour-industrial area of Brindisi (Italy): identification and estimation of the contribution of in-port ship emissions. Sci. Total Environ. 497, 392–400.

Chou, C.C.K., Lee, C.T., Yuan, C.S., Hsu, W.C., Lin, C.Y., Hsu, S.C., Liu, S.C., 2008. Implications of the chemical transformation of Asian outflow aerosols for the long-range transport of inorganic nitrogen species. Atmos. Environ. 42, 7508–7519.

Chow, J.C., Lowenthal, D.H., Chen, L.W.A., Wang, X., Watson, J.G., 2015. Mass reconstruction methods for $PM_{2.5}$: a review. Air Qual. Atmos. & Hlth. 8, 243–263.

Colbeck, I., Harrison, R.M., 1984. Ozone–secondary aerosol–visibility relationships in north-west England. Sci. Total Environ. 34, 87–100.

Ding, H., Liu, Y., Yu, Z., Cheung, C., Zhan, J., 2017. Spatial and temporal characteristics and main contributing regions of high $PM_{2.5}$ pollution in Hong Kong. Aerosol Air Qual. Res. 17, 2955–2965.

Dominick, D., Latif, M.T., Juneng, L., Khan, M.F., Amil, N., Mead, M.I., Nadzir, M.S.M., Moi, P.S., Abu Samah, A., Ashfold, M.J., Sturges, W.T., Harris, N.R.P., Robinson, A.D., Pyle, J.A., 2015. Characterisation of particle mass and number concentration on the east coast of the Malaysian Peninsula during the northeast monsoon. Atmos. Environ. 117, 187–199.

Du, W., Zhang, Y., Chen, Y., Xu, L., Chen, J., Deng, J., Hong, Y., Xiao, H., 2017. Chemical characterization and source apportionment of $PM_{2.5}$ during Spring and Winter in the Yangtze River Delta, China. Aerosol Air Qual. Res. 17, 2165–2180.

Elizabeth, V., Elizabeth, R., Hugo, R., José, G., Gabriela, S., Gerardo, M.V., Uriel, G., Chow, J.C., Watson, J.G., 2004. Analysis of $PM_{2.5}$ and PM_{10} in the atmosphere of Mexico City during 2000-2002. Air Repair. 54, 786–798.

Farren, N.J., Dunmore, R.E., Mead, M.I., Nadzir, M.S.M., Abu Samah, A., Phang, S.-M., Bandy, B.J., Sturges, W.T., Hamilton, J.F., 2019. Chemical characterisation of water-soluble ions in atmospheric particulate matter on the east coast of Peninsular Malaysia. Atmos. Chem. Phys. 19, 1537–1553.

Han, L.H., Zhuang, G.S., Cheng, S.Y., Wang, Y., Li, J., 2007. Characteristics of re-suspended road dust and its impact on the atmospheric environment in Beijing. Atmos. Environ. 41, 7485–7499.

Heo, J.B., Hopke, P.K., Yi, S.M., 2009. Source apportionment of $PM_{2.5}$ in Seoul. Korea. Atmos. Chem. Phys. 9, 4957–4971.

Hsu, S.C., Liu, S.C., Kao, S.J., Jeng, W.L., Huang, Y.T., Tseng, C.M., Tsai, F., Tu, J.Y., Yang, Y., 2007. Water-soluble species in the marine aerosol from the northern South China Sea: High chloride depletion related to air pollution. J. Geophys. Res. 112, D19304.

Hsu, C.Y., Chiang, H.C., Chen, M.J., Chuang, C.Y., Tsen, C.M., Fang, G.C., Tsai, Y.I., Chen, N.T., Lin, T.Y., Lin, S.L., 2017. Ambient $PM_{2.5}$ in the residential area near industrial complexes: Spatiotemporal variation, source apportionment, and health impact. Sci. Total Environ. 590, 204–214.

Hu, M., Slanina, Z.W., Lin, P., Liu, S., Zeng, L., 2008. Acidic gases, ammonia and water-soluble ions in $PM_{2.5}$ at a coastal site in the Pearl River Delta, China. Atmos. Environ. 42, 6310–6320.

Hu, B., Liu, T., Yang, Y., Hong, Y., Li, M., Xu, L., Wang, H., Chen, N., Wu, X., Chen, J., 2019. Characteristics and formation mechanism of surface ozone in a Coastal Island of Southeast China: influence of sea-land breezes and regional transport. Aerosol Air Qual. Res. 19 (8), 1734–1748.

Huang, X.J., Liu, Z.R., Liu, J.Y., Hu, B., Wen, T.X., Tang, G.Q., Zhang, J.K., Wu, F.K., Ji, D.S., Wang, L.L., Wang, Y.S., 2017. Chemical characterization and source identification of $PM_{2.5}$ at multiple sites in the Beijing-Tianjin-Hebei region. China. Atmos. Chem. Phys. 17, 12941–12962.

Hueglin, C., Gehrig, R., Baltensperger, U., Gysel, M., Monn, C., Vonmont, H., 2005. Chemical characterisation of $PM_{2.5}$, PM_{10} and coarse particles at urban, near-city and rural sites in Switzerland. Atmos. Environ. 39, 637–651.

Jennerjahn, T.C., 2012. Biogeochemical response of tropical coastal systems to present and past environmental change. Earth-Sci. Rev. 114, 19–41.

Jeong, J.I., Park, R.J., 2017. Winter monsoon variability and its impact on aerosol concentrations in East Asia. Environ. Pollut. 221, 285–292.

Jia, Y., Rahn, K.A., He, K., Wen, T., Wang, Y., 2008. A novel technique for quantifying the regional component of urban aerosol solely from its sawtooth cycles. J. Geophys. Res. 113, D21309.

Khan, M.F., Shirasuna, Y., Hirano, K., Masunaga, S., 2010. Characterization of $PM_{2.5}$, $PM_{2.5}$–10 and PM > 10 in ambient air, Yokohama. Japan. Atmos. Res. 96, 159–172.

Lee, P.K.H., Brook, J.R., Ewa, D.Z., Mabury, S.A., 2003. Identification of the major sources contributing to $PM_{2.5}$ observed in Toronto. Environ. Sci. Technol. 37, 4831–4840.

Li, W.J., Shao, L.Y., 2009. Observation of nitrate coatings on atmospheric mineral dust particles. Atmos. Chem. Phys. 9, 1863–1871.

Li, T.C., Yuan, C.S., Huang, H.C., Lee, C.L., Wu, S.P., Tong, C., 2016. Inter-comparison of seasonal variation, chemical characteristics, and source identification of atmospheric fine particles on both sides of the Taiwan strait. Sci. Rep. 6, 22956.

Li, M., Hu, M., Du, B., Guo, Q., Tan, T., Zheng, J., Huang, X., He, L., Wu, Z., Guo, S., 2017. Temporal and spatial distribution of $PM_{2.5}$ chemical composition in a coastal city of Southeast China. Sci. Total Environ. 605-606, 337–346.

Li, M., Hu, M., Guo, Q., Tan, T., Du, B., Huang, X., He, L., Guo, S., Wang, W., Fan, Y., Xu, D., 2018. Seasonal source apportionment of $PM_{2.5}$ in Ningbo, a Coastal City in Southeast China. Aerosol Air Qual. Res. 18, 2741–2752.

Liu, Q.Y., Baumgartner, J., Zhang, Y.X., Schauer, J.J., 2016. Source apportionment of Beijing air pollution during a severe winter haze event and associated pro-inflammatory responses in lung epithelial cells. Atmos. Environ. 126, 28–35.

Liu, B., Song, N., Dai, Q., Mei, R., Sui, B., Bi, X., Feng, Y., 2016a. Chemical composition and source apportionment of ambient $PM_{2.5}$ during the non-heating period in Taian. China. Atmos. Res. 170, 23–33.

Liu, B., Li, T., Yang, J., Wu, J., Wang, J., Gao, J., Bi, X., Feng, Y., Zhang, Y., Yang, H., 2017. Source apportionment and a novel approach of estimating regional contributions to ambient $PM_{2.5}$ in Haikou. China. Environ. Pollut. 223, 334–345.

Liu, W., Xu, Y., Liu, W., Liu, Q., Yu, S., Liu, Y., Wang, X., Tao, S., 2018. Oxidative potential of ambient $PM_{2.5}$ in the coastal cities of the Bohai Sea, northern China: Seasonal variation and source apportionment. Environ. Pollut. 236, 514–528.

Luo, J.Q., Du, P.J., Samat, A., Xia, J.S., Che, M.Q., Xue, Z.H., 2017. Spatiotemporal pattern of $PM_{2.5}$ concentrations in mainland china and analysis of its influencing factors using geographically weighted regression. Scientific Reports 7, 40607.

Martens, C.S., Wesolowski, J.J., Harriss, R.C., Kaifer, R., 1973. Chlorine loss from Puerto Rican and San Francisco Bay area marine aerosols. J. Geophys. Res. 78, 8778–8792.

Mcculloch, A., Aucott, M.L., Benkovitz, C.M., Graedel, T.E., Kleiman, G., Midgley, P.M., Li, Y.F., 1999. Global emissions of hydrogen chloride and chloromethane from coal combustion, incineration and industrial activities: Reactive Chlorine Emissions Inventory. J. Geophys. Res. 104, 8391–8403.

Moffet, R.C., Desyaterik, Y., Hopkins, R.J., Tivanski, A.V., Gilles, M.K., Wang, Y., Shutthanandan, V., Molina, L.T., Abraham, R.G., Johnson, K.S., 2008. Characterization of aerosols containing Zn, Pb, and Cl from an industrial region of Mexico City. Environ. Sci. Technol. 42, 7091.

Morawska, L., Zhang, J.J., 2002. Combustion sources of particles. 1. Health relevance and source signatures. Chemosphere. 49, 1045–1058.

Norris, G., Duvall, R., Brown, S., Bai, S., 2014. EPA positive matrix factorization PMF5.0 fundamentals and user guide.

Paatero, P., 1997. Least squares formulation of robust non-negative factor analysis[J]. Chemom. Intell. Lab. Syst. 37 (1), 23–35.

Paatero, P., Hopke, P.K., 2003. Discarding or down weighting high-noise variables in factor analytic models. Anal. Chim. Acta 490, 277–289.

Paatero, P., Tapper, U., 1994. Positive matrix factorization: a non-negative factor model with optimal utilization of error estimates of data values[J]. Environmetrics 5 (2), 111–126.

Polissar, A.V., Hopke, P.K., Paatero, P., Malm, W.C., Sisler, J.F., 1998. Atmospheric

aerosol over Alaska: 2 elemental composition and sources. J. Geophys. Res. 103, 19045–19057.
Poschl, U., 2005. Atmospheric aerosols: composition, transformation, climate and health effects. Angew. Chem. Int. Edit. 44, 7520–7540.
Querol, X., Alastuey, A., Viana, M.M., Rodriguez, S., Artiñano, B., Salvador, P., Santos, S.G.D., Patier, R.F., Ruiz, C.R., Rosa, J.D.L., 2004. Speciation and origin of PM_{10} and $PM_{2.5}$ in Spain. J. Aerosol Sci. 35, 1151–1172.
Quinn, P.K., Bates, T.S., Coffman, D.J., Miller, T.L., Johnson, J.E., Covert, D.S., Putaud, J.P., Neusüß, C., Novakov, T., 2000. A comparison of aerosol chemical and optical properties from the 1st and 2nd aerosol characterization experiments. Tellus B. 52, 239–257.
Safai, P.D., Raju, M.P., Rao, P.S.P., Pandithurai, G., 2014. Characterization of carbonaceous aerosols over the urban tropical location and a new approach to evaluate their climatic importance. Atmos. Environ. 92, 493–500.
Seo, J., Kim, J.Y., Youn, D., Lee, J.Y., Kim, H., Lim, Y.B., Kim, Y., Jin, H.C., 2017. On the multiday haze in the Asian continental outflow: the important role of synoptic conditions combined with regional and local sources. Atmos. Chem. Phys. 17, 9311–9332.
Shi, G.-L., Tian, Y.-Z., Zhang, Y.-F., Ye, W.-Y., Li, X., Tie, X.-X., Feng, Y.-C., Zhu, T., 2011. Estimation of the concentrations of primary and secondary organic carbon in ambient particulate matter: Application of the CMB-Iteration method. Atmos. Environ. 45, 5692–5698.
Song, Y., Zhang, Y., Xie, S., Zeng, L., Zheng, M., Salmon, L.G., Shao, M., Slanina, S., 2006. Source apportionment of $PM_{2.5}$ in Beijing by positive matrix factorization. Atmos. Environ. 40, 1526–1537.
Sun, Y., Zhuang, G., Tang, A.A., Wang, Y., An, Z., 2006. Chemical characteristics of $PM_{2.5}$ and PM_{10} in haze-fog episodes in Beijing. Environ. Sci. Technol. 40, 3148–3155.
Tao, J., Gao, J., Zhang, L., Zhang, R., Che, H., Zhang, Z., Lin, Z., Jing, J., Cao, J., Hsu, S.C., 2014. $PM_{2.5}$ pollution in a megacity of southwest China: source apportionment and implication. Atmos. Chem. Phys. 14, 8679–8699.
Turpin, B.J., Huntzicker, J.J., 1995. Identification of secondary organic aerosol episodes and quantitation of primary and secondary organic aerosol concentrations during SCAQS. Atmos. Environ. 29, 3527–3544.
Wang, H., Shooter, D., 2001. Water soluble ions of atmospheric aerosols in three New Zealand cities: seasonal changes and sources. Atmos. Environ. 35 (34), 6031–6040.
Wang, H., Tan, S.-C., Wang, Y., Jiang, C., Shi, G.-Y., Zhang, M.-X., Che, H.-Z., 2014. A multisource observation study of the severe prolonged regional haze episode over eastern China in January 2013. Atmos. Environ. 89, 807–815.
Wang, Y., Jia, C., Tao, J., Zhang, L., Liang, X., Ma, J., Gao, H., Huang, T., Zhang, K., 2016. Chemical characterization and source apportionment of $PM_{2.5}$ in a semi-arid and petrochemical-industrialized city, Northwest China. Sci. Total Environ. 573, 1031–1040.
Wang, B., Chen, Y., Zhou, S., Li, H., Wang, F., Yang, T., 2019. The influence of terrestrial transport on visibility and aerosol properties over the coastal East China Sea. Sci. Total Environ. 649, 652–660.
Watson, J.G., Chow, J.C., Houck, J.E., 2001. $PM_{2.5}$ chemical source profiles for vehicle exhaust, vegetative burning, geological material, and coal burning in Northwestern Colorado during 1995. Chemosphere. 43, 1141–1151.
Weagle, C.L., Snider, G., Li, C., van Donkelaar, A., Philip, S., Bissonnette, P., Burke, I., Jackson, J., Latimer, R., Stone, E., Abboud, I., Akoshile, C., Nguyen Xuan, A., Brook, J.R., Cohen, A., Dong, J., Gibson, M.D., Griffith, D., He, K.B., Holben, B.N., Kahn, R., Keller, C.A., Kim, J.S., Lagrosas, N., Lestari, P., Khian, Y.L., Liu, Y., Marais, E.A., Martins, J.V., Misra, A., Muliane, U., Pratiwi, R., Quel, E.J., Salam, A., Segey, L., Tripathi, S.N., Wang, C., Zhang, Q., Brauer, M., Rudich, Y., Martin, R.V., 2018. Global sources of fine particulate matter: interpretation of $PM_{2.5}$ chemical composition observed by SPARTAN using a global chemical transport model. Environ. Sci. Technol. 52, 11670–11681.
Webster, P.J., Magana, V.O., Palmer, T.N., Shukla, J., Tomas, R.A., Yanai, M., Yasunari, T., 1998. Monsoons: Processes, predictability, and the prospects for prediction. J. Geophys. Res-Oceans. 103, 14451–14510.
Xu, L., Jiao, L., Hong, Z., Zhang, Y., Du, W., Wu, X., et al., 2018. Source identification of $PM_{2.5}$, at a port and an adjacent urban site in a coastal city of China: impact of ship emissions and port activities. Sci. Total Environ. 634, 1205–1213.
Yeh, C.-F., Lee, C.-L., Brimblecombe, P., 2017. Effects of seasonality and transport route on chemical characteristics of $PM_{2.5}$ and $PM_{2.5\text{-}10}$ in the East Asian Pacific Rim Region. Aerosol Air Qual. Res. 17, 2988–3005.
Yin, L., Niu, Z., Chen, X., Chen, J., Zhang, F., Xu, L., 2014. Characteristics of water-soluble inorganic ions in $PM_{2.5}$ and $PM_{2.5}$-10 in the coastal urban agglomeration along the Western Taiwan Strait Region, China. Environ. Sci. Pollut. Res. Int. 21, 41–56.
Ying, Q., Wu, L., Zhang, H., 2014. Local and inter-regional contributions to $PM_{2.5}$ nitrate and sulfate in China. Atmos. Environ. 94, 582–592.
Zárate, I.O.D., Ezcurra, A., Lacaux, J.P., Dinh, P.V., 2000. Emission factor estimates of cereal waste burning in Spain. Atmos. Environ. 34, 3183–3193.
Zhang, M., Gao, L., Ge, C., Xu, Y., 2007. Simulation of nitrate aerosol concentrations over East Asia with the model system RAMSCMAQ. Tellus 59, 372–380.
Zhang, L., Liao, H., Li, J., 2010. Impacts of Asian summer monsoon on seasonal and interannual variations of aerosols over eastern China. J. Geophys. Res. 115, D00K05.
Zhang, F.W., Xu, L.L., Chen, J.S., Yu, Y.K., Niu, Z.C., Yin, L.Q., 2012. Chemical compositions and extinction coefficients of $PM_{2.5}$ in peri-urban of Xiamen, China, during June 2009–May 2010. Atmos. Res. 106, 155–158.
Zhang, R., Jing, J., Tao, J., Hsu, S.C., Wang, G., Cao, J., Lee, C.S.L., Zhu, L., Chen, Z., Zhao, Y., Shen, Z., 2013. Chemical characterization and source apportionment of $PM_{2.5}$ in Beijing: seasonal perspective. Atmos. Chem. Phys. 13, 7053–7074.
Zhang, Y., Zhang, H., Deng, J., Du, W., Hong, Y., Xu, L., Qiu, Y., Hong, Z., Wu, X., Ma, Q., Yao, J., Chen, J., 2017. Source regions and transport pathways of $PM_{2.5}$ at a regional background site in East China. Atmos. Environ. 167, 202–211.
Zhao, P., Dong, F., Yang, Y., He, D., Zhao, X., Zhang, W., Yao, Q., Liu, H., 2013. Characteristics of carbonaceous aerosol in the region of Beijing, Tianjin, and Hebei, China. Atmos. Environ. 71, 389–398.
Zheng, L., Yang, X., Lai, S., Ren, H., Yue, S., Zhang, Y., Huang, X., Gao, Y., Sun, Y., Wang, Z., Fu, P., 2018. Impacts of springtime biomass burning in the northern Southeast Asia on marine organic aerosols over the Gulf of Tonkin, China. Environ. Pollut. 237, 285–297.
Zhou, J., Xing, Z., Deng, J., Du, K., 2016. Characterizing and sourcing ambient $PM_{2.5}$ over key emission regions in China I: Water-soluble ions and carbonaceous fractions. Atmos. Environ. 135, 20–30.
Zíková, N., Wang, Y., Yang, F., Li, X., Tian, M., Hopke, P.K., 2016. On the source contribution to Beijing $PM_{2.5}$ concentrations. Atmos. Environ. 134, 84–95.